

Article

Effect of Expansion Deformation on the Mechanical Properties and Corrosion Resistance of an AISI 304 Stainless Steel Tube in Water from an Oilfield

Xiaoming Ren ¹, Wenfei Yang ¹, Lidong He ¹, Dejun Li ^{2,*} and Juntao Yuan ²¹ The Ninth Oil Production of Petrochina Changqing Oilfield Company, Yinchuan 750006, China² CNPC Tubular Goods Research Institute, Xi'an 710077, China

* Correspondence: lidejun352@cnpc.com.cn

Abstract: The effects of expansion deformation on the mechanical properties and corrosion resistance of an AISI 304 stainless steel (SS) tube with dimensions of ϕ 108 mm \times 6 mm were studied with a full-scale test, a mechanical property test, microstructural analysis and a corrosion property test in order to explore the feasibility of using AISI 304 SS tubes as solid expandable tubes in repairing damaged well casings. The results showed that the AISI 304 SS tube had good expansion performance, suitable strength after expansion and excellent corrosion resistance, and it met the technical requirements for repairing the casings of common oil wells. After \sim 11% radial expansion, the internal pressure strength and collapsing strength of the tube were 71 and 32 MPa, respectively. The increase in dislocations, and in the formation of strain-induced martensite and twinning stimulated by plastic deformation, led to the yield strength of the AISI 304 SS tube increasing from 249 to 539 MPa; however, the corrosion resistance of the AISI 304 SS tube was somewhat worsened because of the increase in dislocations and strain-induced martensite caused by expansion deformation. However, the corrosion resistance of the AISI 304 SS tube was still much better than that of conventional casings.

Keywords: AISI 304 stainless steel; solid expandable tube; strain-induced martensite; corrosion resistance



Citation: Ren, X.; Yang, W.; He, L.; Li, D.; Yuan, J. Effect of Expansion Deformation on the Mechanical Properties and Corrosion Resistance of an AISI 304 Stainless Steel Tube in Water from an Oilfield. *Coatings* **2022**, *12*, 1415. <https://doi.org/10.3390/coatings12101415>

Academic Editors: Paolo Castaldo and Giorgos Skordaris

Received: 20 July 2022

Accepted: 26 September 2022

Published: 27 September 2022

Publisher's Note: MDPI stays neutral with regard to jurisdictional claims in published maps and institutional affiliations.



Copyright: © 2022 by the authors. Licensee MDPI, Basel, Switzerland. This article is an open access article distributed under the terms and conditions of the Creative Commons Attribution (CC BY) license (<https://creativecommons.org/licenses/by/4.0/>).

1. Introduction

Solid expandable tube (SET) technology is known to be the most revolutionary innovation technology for drilling and completing wells. It has been used successfully for slim hole casing designs and for handling the abnormal pressures encountered downhole during drilling. In addition, this technology has been used to rejuvenate well bores for the deepening of wells, for casing repair and in sidetrack drilling for stimulation. The diameters of SETs need to be expanded by \sim 10% or even by 30% [1,2] downhole through the action of hydraulic pressure or mechanical force, and then the inner diameter of the well bore must be returned to the maximum size. The tube material is one of the key technologies for SETs and has been a research hotspot in this area. In order to obtain tubes that are easy to expand and have enough strength after expansion, researchers have extensively screened various existing pipes, especially in recent years with the increasing maturity of advanced steel technologies, such as dual phase (DP) steels, transformation-induced plasticity (TRIP) steels and high-Mn twinning-induced plasticity (TWIP) steels, which are considered to have good application prospects in the field of SET production. The above-mentioned research on SET materials has mainly considered mechanical properties; however, the corrosion resistance of tube materials should also be considered in actual SET applications, as many instances of casing damage are caused by corrosion. In particular, when the casing damage caused by corrosion is repaired using SET technology, the corrosion resistance of the SET directly determines the service life of the well after repair.

AISI 304 stainless steel (SS) is a universal stainless steel with excellent, comprehensive properties, and it is one of the most widely used Cr-Ni series austenitic stainless steels [3].

AISI 304 SS has moderate strength and good ductility and corrosion resistance, and it thus seems to be an ideal raw material for manufacturing anti-corrosion SETs. Unlike a regular casing, a SET must undergo radial plastic deformation in the well bore before formal service. Many researchers have shown that the microstructure, dislocation density, texture and residual stress of AISI 304 SS undergo remarkable changes after plastic deformation, resulting in a decrease in the corrosion resistance [4,5]. It is well-known that the dislocation density and texture change during plastic deformation, microstructural transformation occurs because of the low stacking fault energy (SFE) of AISI 304 SS and then strain-induced martensite is formed in an austenite matrix [6,7]. Related research has shown that the corrosion rate of AISI 304 SS after plastic deformation is proportional to the strain-induced martensite content because martensite has higher electrochemical activity than austenite [4,5,8,9]. Besides the martensite content, other factors can also influence the corrosion behavior of AISI 304 SS after plastic deformation. For example, the dislocation density, grain size, grain size distribution [10] and texture [5] can also play important roles. Expansion deformation doubtless also leads to changes in the mechanical properties and microstructural characteristics of AISI 304 SS tubes, and thus its corrosion resistance will be affected. Although the certainty of this influence has already been proven in many previous studies, severe plastic deformation methods, such as low temperature and large strain rolling or torsion, were often used in such research, which are very different from the plastic deformation of SETs. Moreover, few reports on plastic deformation at normal temperatures and low strain similar to those of SETs have been published, but this type of problem has very important engineering applications. After all, AISI 304 SS can obtain ultra-fine grain, strong texture and sufficient phase transformation, surface strengthening and compressive stress through common plastic deformations, all of which can also be easily achieved through severe plastic deformation to improve the mechanical properties, friction performance and corrosion resistance [3,8].

The research in this study is put forward against the background of actual applications, and the feasibility of AISI 304 SS tubes used as SETs is discussed in terms of the expansion pressure, internal pressure and collapse strength of the tubes after expansion deformation and corrosion treatment. In this study, an as-manufactured AISI 304 SS tube was expanded on an expansion tester designed in-house, and then the microstructural evolution, mechanical properties and corrosion resistance of the AISI 304 SS tube before and after expansion deformation were tested. In particular, its corrosion behavior in a sample of water from an oilfield in China was studied in detail. It is hoped that this study can provide a theoretical basis and technical support for the application of AISI 304 SS in SETs.

2. Experimental Procedures

Casings with dimensions of ϕ 139.7 mm \times 7.72 mm are often used as production casings, and the corresponding SETs with dimensions of ϕ 108 mm \times 3–7 mm are used to repair the damaged casings; therefore, an AISI 304 SS tube with dimensions of ϕ 108 mm \times 6 mm was taken as the research object. The chemical composition of the experimental tube is listed in Table 1.

Table 1. Chemical composition of AISI 304 stainless steel tube.

Element	C	Si	Mn	P	S	Cr	Ni	Mo	Cu	Fe
wt.%	0.042	0.39	1.15	0.039	0.0033	18.21	8.15	0.087	0.36	Bal.

A 2.5 m long 304 SS tube was expanded by water pressure in an expansion test machine designed in-house, similar to how a SET is actually installed in a well. An expansion cone with an outer diameter of 105 mm was set inside one end of the experimental tube and driven by hydraulic pressure to move to the other end; as a result, the diameter of the experimental tube was expanded. After expansion, the outer diameter and thickness of the tube were measured with Vernier calipers and an ultrasonic thickness gauge, and the

average values of the outer diameter and thickness were 118.20 and 5.80 mm, respectively; thus, the expansion rate of the inner diameter was determined to be ~11%. The expansion rate is the ratio of the increase in the inner diameter to the original inner diameter. The final internal pressure and collapse strength of the tube after expansion were tested at room temperature according to the API RP 5C5 standard, and the test pressure medium was water. The length of the sample tubes used for the full-scale physical test of internal pressure strength and collapse strength was not less than eight times the outer diameter, in accordance with the requirements of the API RP 5C5 standard.

The phase compositions of the 304 SS tube before and after expansion were determined using a Bruker D8A X-ray diffractometer (Bruker, Karlsruhe, Germany) with Cu-K α radiation. The scanning angle range was set from 35° to 105° with a step of 0.02°. The tube voltage and current were 40 kV and 40 mA, respectively. Thin-sheet specimens with a thickness of 0.5 mm were cut from the tubes before and after expansion, and the sampling position was near the inner wall and at a tangent to it. The specimens' thicknesses were modified to 30–50 μ m by polishing them with sandpaper, and round foils with a diameter of 3 mm were punched out. The foils were prepared as transmission electron microscopy specimens by twin-jet electropolishing. The microstructural characteristics of the AISI 304 SS before and after expansion were observed with a JEOL 2100 transmission electron microscope (JEOL, Tokyo, Japan).

Tensile specimens with a width of 25.4 mm and gauge length of 50 mm were cut from the experimental tubes. Uniaxial tensile testing was carried out on an UTM5305 tensile tester (Suns, Shenzhen, China) at a tensile rate of 3 mm/min, in accordance with the ASTM A370-19^{e1} standard, and then the yield strength (0.5% EUL), tensile strength and elongation of the AISI 304 SS tube before and after expansion were obtained.

Restricted by the size of the experimental tubes, three half-size specimens with a length of 55 mm, a height of 10 mm and a width of 5 mm were machined as a group for Charpy V-notch impact testing from expanded and unexpanded tubes along the longitudinal direction. The impact test was carried out on a PIT 752D-2 impact tester (WANCE, Shenzhen, China) at 0 °C, and the impact absorption energies of the AISI 304 SS tubes before and after expansion were measured. The average of three specimens in each state was recorded as the testing result. The hardness values of the AISI 304 SS tubes before and after expansion were measured with an RB2002T Rockwell hardness tester (Wilson, Boston, MA, USA), and the average of five test points was taken as the hardness testing result.

Plate specimens with a length of 10 mm, a width of 10 mm and a thickness of 3 mm for the electrochemical test were cut from the tubes before and after expansion, and the sampling position was near the inner wall and at a tangent to the inner wall. The test surface was then successively polished with coarse to fine sandpaper. The solution used for the electrochemical test was water collected from a particular oil well, and the results of the composition analysis of the water are listed in Table 2. A gas composed of 40 vol.% CO₂ and 60% N₂ was continuously injected into the test solution in order to simulate the actual conditions of an oil well. The electrochemical tests were carried out on a CS350 electrochemical workstation (CorrTest, Wuhan, China). The working electrode was the test material. As well as the test surface, the remaining surfaces of the electrochemical specimens were sealed with epoxy resin. The counter-electrode was a platinum plate, and an Ag/AgCl electrode was used as the reference electrode.

Table 2. Composition analysis results for the test solution.

Ionic Species (mg/L)	K ⁺	Na ⁺	Ca ²⁺	Mg ²⁺	HCO ₃ ⁻	Cl ⁻	SO ₄ ²⁻
Produced water	7286.8	11,785.2	3075.21	319.06	701.56	30,694.6	149.75

Before the electrochemical test, the electrochemical specimen was immersed in the test solution for 1 h in order to ensure the stability of the open-circuit voltage. The frequency measurement range of the electrochemical impedance spectroscopy was from 0.01

to 100,000 Hz, and the amplitude was 5 mV. The impedance spectrum data were fitted in ZsimpWin software (P/N1109082–Rev.A, AMETEK, Oka Ridge, TN, USA). The measurement range of the polarization curve was -1.15 to -0.3 V, and the scanning rate was 0.001 v/s. The test temperature was 60 °C.

Simulation tests of corrosion resistance for unexpanded and expanded AISI 304 SS tubes were carried out on an autoclave. For this, corrosion samples with a length of 40 mm, a width of 10 mm and a thickness of 3 mm were cut as a group from the tubes before and after expansion along the longitudinal direction of the tube body. For comparison, identical corrosion samples were cut from a common J55 casing. Before testing, all samples were successively polished by coarse to fine sandpaper. The test temperature was set at 60 °C; the total pressure and partial pressure of CO_2 were 2 and 0.04 MPa, respectively; and the test period was 240 h. The solution in the autoclave was consistent with the solution in the electrochemical test, which was water taken from a particular oil well. All samples were weighed before and after testing to determine the corrosion rate of AISI 304 SS, especially for the samples after testing. The corrosion scales were removed and the samples were dried before weighing.

3. Results

3.1. Full-Scale Testing

The curve for the expansion pressure vs. displacement measured during the hydraulic expansion of the AISI 304 SS tube is shown in Figure 1. It must be pointed out that expansion pressure is an important parameter for measuring the service performance of SETs. Field operators always hope that the expansion pressure can be maintained below 30 MPa to reduce the load on the pressure equipment and pipeline and ensure the safety of the operation. It can be seen from Figure 1 that the expansion pressure of the AISI 304 SS tube was always maintained below 23 MPa during the entire expansion process. In addition to the expansion pressure, the internal pressure strength and collapse strength of the expanded SET are also important performance parameters that determine the bearing capacity of the casing after repairs. The full-scale test results showed that the final internal pressure and collapse strength of the AISI 304 SS tube after expansion were 71 and 32 MPa, respectively.

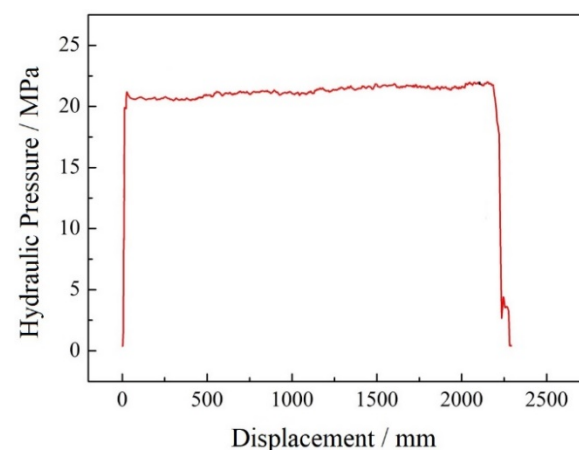


Figure 1. The curve for hydraulic pressure vs. displacement during the expansion of the AISI 304 SS tube.

3.2. Microstructure and Mechanical Properties

The X-ray diffraction (XRD) spectra of the AISI 304 SS tube before and after expansion are presented in Figure 2. It can be seen that the microstructure of the as-manufactured AISI 304 SS tube was composed of austenite and α' -martensite, and austenite was the main part. After expansion, the intensity of the existing diffraction peak of the α' -martensite increased further, and several new diffraction peaks for α' -martensite could be found in the XRD

patterns of the expanded tube, indicating that strain-induced martensite transformation had occurred in the steel during expansion deformation, which is often the case during the plastic deformation of AISI 304 SS.

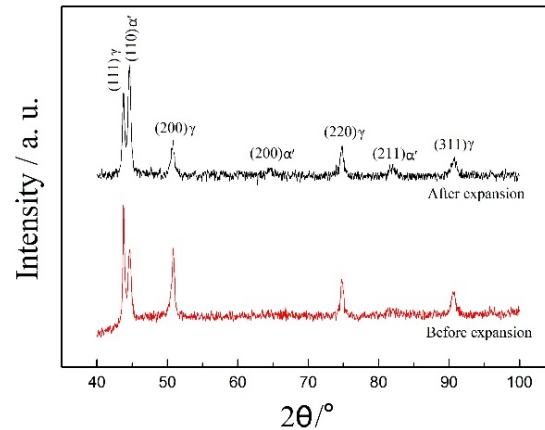


Figure 2. XRD patterns for AISI 304 SS tube before and after expansion.

The microstructure of the AISI 304 SS before and after expansion is shown in Figure 3. Before expansion, the dislocations in the austenitic matrix were sparse and the dislocation density was low because the AISI 304 SS tubes were solution-treated before leaving the factory, as shown in Figure 3a. However, a large number of stacking faults can be observed on the austenitic matrix because of the low SFE of the AISI 304 SS, and the dislocation density in the austenite near the stacking fault was also very low, as shown in Figure 3b. After expansion, the dislocation density in the austenitic matrix of 304 SS increased significantly, shear bands formed in grains and a large number of mechanical twins formed near the stacking faults, as shown in Figure 3c,d.

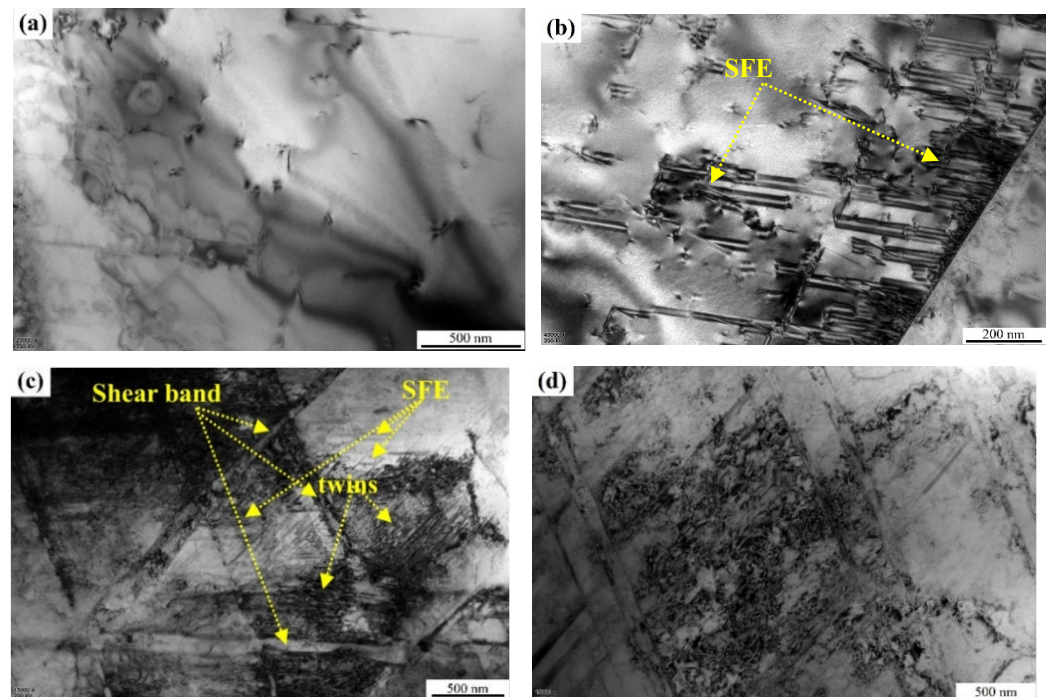


Figure 3. TEM images of AISI 304 SS before and after expansion: (a,b) before expansion; (c,d) after expansion.

The stress–strain curves obtained from the tensile test of AISI 304 SS before and after expansion are shown in Figure 4. Whether expanded or not, the stress–strain curves of

ASIS 304 SS present continuous yield characteristics. After expansion, the strength and hardness of the steel increased significantly, and its plasticity and toughness decreased. The mechanical properties of the AISI 304 SS before and after expansion are shown in Table 3. Although the expansion rate of the ASIS 304 SS tube was only 11%, the strength indices of the steel increased greatly because of its excellent work-hardening ability. The yield strength increased from 249 to 539 MPa, the tensile strength increased from 633 to 735 MPa and the hardness increased slightly from 79 to 94 HRB. However, the indices of plasticity and toughness decreased slightly, the elongation decreased from 62.5% to 45% and the impact absorbed energy decreased from 133 to 117 J.

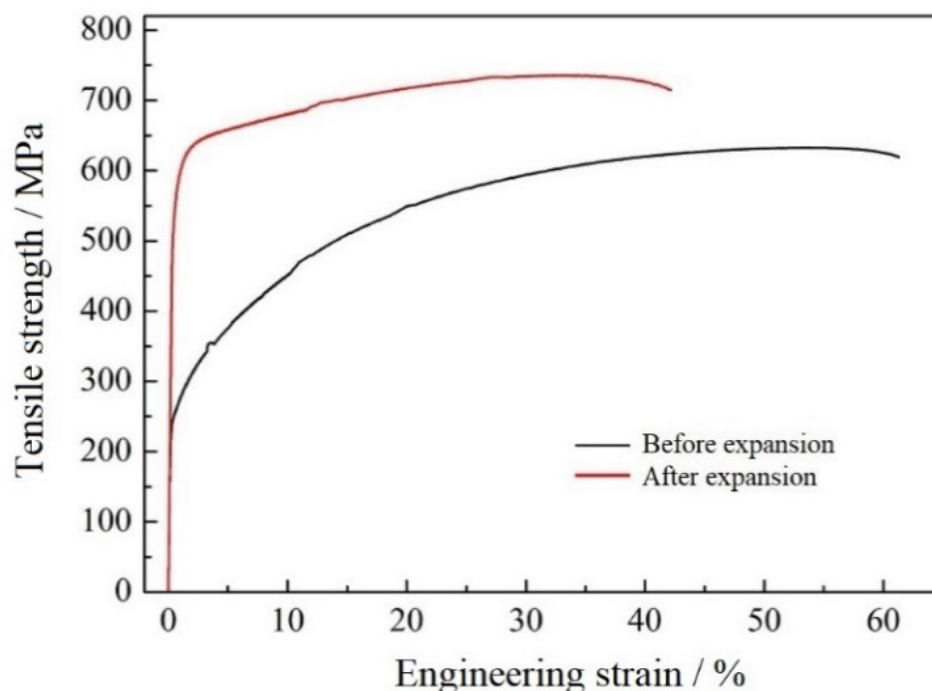


Figure 4. Stress–strain curves of AISI 304 SS before and after expansion.

Table 3. Mechanical properties of AISI 304 SS before and after expansion.

State	Tensile Strength (MPa)	Yield Strength (MPa)	Elongation (%)	Rockwell Hardness (HRB)	Impact Absorbed Energy (J)
Before expansion	633	249	62.5	79	133
After expansion	735	539	45.0	94	117

3.3. Polarization Curves

The polarization curves of the AISI 304 SS in water from an oil well before and after expansion are shown in Figure 5. The anodic polarization curve shows that the expansion deformation led to several obvious changes in the passivation zone of the AISI 304 SS. The corrosion potential E_{corr} , the corrosion current density I_{corr} and the breakdown potential E_b of the AISI 304 SS before and after expansion were determined with the Tafel slope extrapolation method. It was found that there was no obvious change in the corrosion potential of AISI 304 SS compared with before expansion, but a remarkable increase in the corrosion current density occurred. The corrosion current density of the AISI 304 SS increased from 0.97 to $2.93 \mu\text{A}\cdot\text{cm}^{-2}$ after expansion.

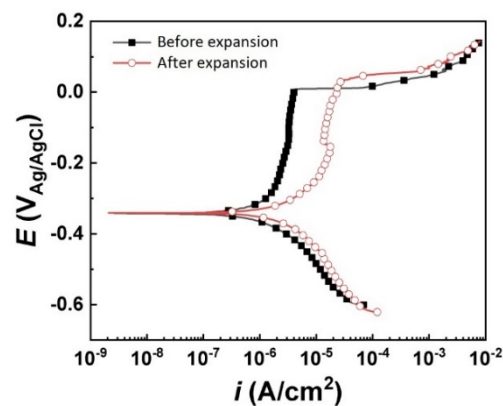


Figure 5. Polarization curves of AISI 304 SS before and after expansion in the test solution.

3.4. Electrochemical Impedance Spectrum

The electrochemical impedance spectra (EIS) before and after expansion were measured, and then a Nyquist diagram, the phase angle and a Bode diagram were produced in order to further clarify the corrosion mechanism of AISI 304 SS in oilfield water, as shown in Figure 6. The Nyquist curves of AISI 304 SS before and after expansion had similar characteristics; namely, a single capacitive reactance arc in the first quadrant. Expansion resulted in a decrease in the radius of the capacitive reactance arc, and the impedance modulus of AISI 304 SS decreased from $15,262 \Omega \cdot \text{cm}^2$ before expansion to $6766 \Omega \cdot \text{cm}^2$. This means that the expansion deformation increased the corrosion reaction rate of AISI 304 SS and reduced the corrosion resistance of the steel in the water from the oilwell. Moreover, the Bode diagram for the AISI 304 SS before expansion was located above the Bode diagram from after expansion, which also means that the impedance modulus and the corrosion resistance of 304 stainless steel both decreased after expansion.

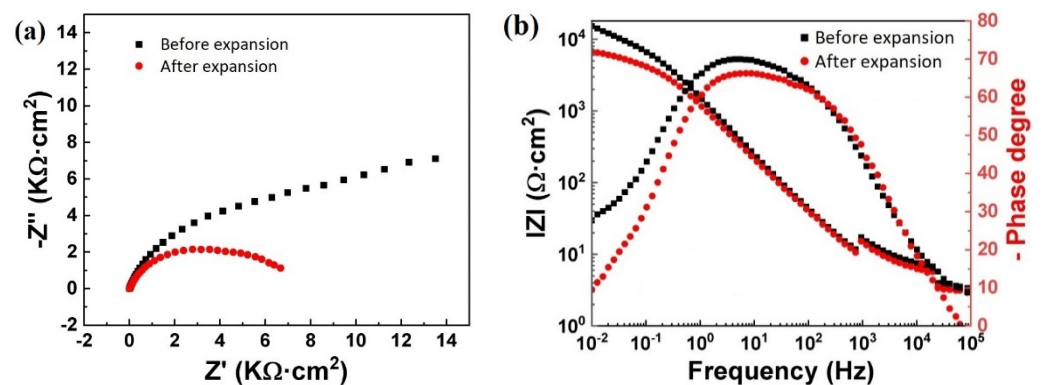


Figure 6. Impedance spectra (a) and Bode diagrams (b) of AISI 304 SS before and after expansion in the test solution.

3.5. Corrosion Simulation Test in Autoclave

It can be seen from the results of the 240 h corrosion simulation test in an autoclave that the corrosion rates of the unexpanded and expanded 304 SS were 0.018 and 0.0224 mm/a, respectively; moreover, no obvious pitting corrosion features could be found on the surface of the tested samples, as shown in Figure 7. Although the expansion deformation led to a clear increase in the corrosion rate of the 304 SS, the corrosion resistance of the expanded 304 SS tube was still better than that of the common J55 casing under the same testing conditions: the corrosion rate of the common J55 casing reached 0.0442 mm/a; corrosion pits could be observed on the surface of the tested samples, as shown in Figure 8; and the pitting corrosion rate reached 0.098 mm/a.

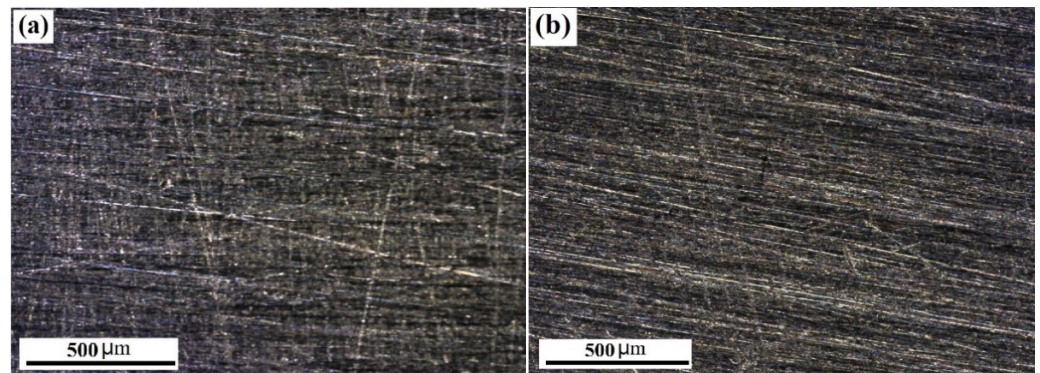


Figure 7. Surface morphology of corrosion coupons of AISI 304 SS: (a) before expansion; (b) after expansion.

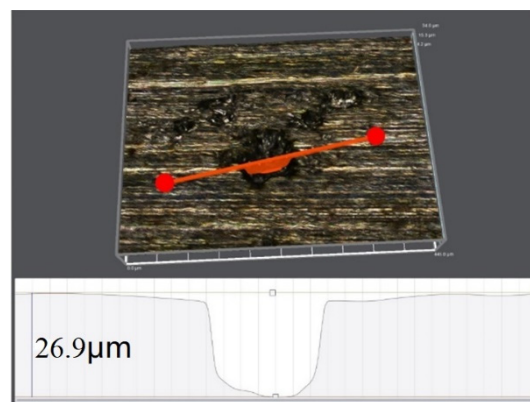


Figure 8. Corrosion pit morphology of common J55 casing after the corrosion simulation test.

4. Discussion

Firstly, the yield strength of the AISI 304 SS increased by 116% after an expansion deformation at an inner diameter expansion rate of ~11%. AISI 304 SS is a typical Cr-Ni austenitic SS with a low SFE [4]. Previous research has shown that metals with low SFEs have higher work-hardening abilities than metals with high SFEs. The stability of stacking fault structures in metals is inversely proportional to the SFE of the materials. The SFE value of the AISI 304 SS used in this study was calculated to be 24.66 mJ/m^2 using the equation proposed in [11], and the SFE value of $\alpha\text{-Fe}$ was $\sim 250 \text{ mJ/m}^2$, so a large number of stacking fault structures could be observed in the microstructure of the AISI 304 SS, as shown in Figure 3b. In reducing the system's energy, a perfect dislocation in face-centered cubic metals often splits two or more partial dislocations and stacking faults to form extended dislocations [12]. It is well-known that dislocation slippage is the most important mechanism for the plastic deformation of metal materials, even if the mechanisms of twinning and phase transformation must occur with the help of dislocation slippage as well. Karaman et al. believe that the stacking fault structure is the precursor of mechanical twinning [13,14] and the core of martensite nucleation [13]. Extended dislocation in metals with a low SFE is difficult to condense into perfect dislocation, with the inverse being the case for cross-slipping, because of the existence of a stable stacking fault structure caused by the low SFE; thus, the extended dislocation can only result in planar slipping on the $\{111\}$ planes. These demonstrate stronger interactions between the extended dislocation and the existing dislocations during planar slipping, and the stress concentration levels of the dislocations near the obstacles in low-SFE metals are higher than those in high-SFE metals. However, the mechanisms of twinning and/or phase transformation can be stimulated, resulting in a stronger work-hardening ability for low-SFE metals. It can be seen from Figure 3d that a large number of mechanical twins can be observed near the stacking faults. The yield strength increased from 249 to 539 MPa, the tensile strength increased from 633

to 735 MPa and the hardness increased slightly from 79 to 94 HRB when the inner diameter of the AISI 304 SS tube used in this study was expanded by ~11%.

Secondly, the results of the full-scale expansion test showed that the AISI 304 SS tube with an outer diameter of 108 mm and a thickness of 6 mm had good expansion performance because an expansion pressure of less than 23 MPa could easily expand its diameter to the design size, and the expansion pressure was stable throughout the whole test process. The expansion pressure is a key parameter for characterizing the expansion performance of a SET. Considering the safety of oilfield operations, field installers always want to reduce the expansion pressure of SETs as much as possible. Previous research has shown that many factors, such as the yield strength, work-hardening ability and dimensions of the SET; the geometric configuration of the expansion tool; the expansion ratio; and the lubrication conditions between the outer surface of the expansion cone and the inner wall of the SET, can affect the expansion pressure of the SET. Obviously, lower yield strength can effectively reduce the expansion pressure of a SET, which was one of the most direct reasons for selecting the AISI 304 SS tube as the research object in this study. Moreover, the internal pressure and collapse strength of the AISI 304 SS tube after 11% expansion were 71 and 31 MPa, respectively, meeting the technical requirements of casing repairs in common oil wells. After all, the test pressure of well bores' is not generally higher than 30 MPa when repairing damaged well casings, and the working pressure is lower than the test pressure.

Thirdly, the results of the electrochemical and corrosion simulation tests showed that expansion deformation could degrade the corrosion resistance of AISI 304 SS in the water from an oilfield. Previous research has shown that the corrosion behavior of AISI 304 SS is related to the stress state, dislocation density, chloride ion concentration and so on [15]. The AISI 304 SS after solid-solution treatment presented a single austenite microstructure with a dislocation density of $\sim 10^6/\text{cm}^2$, and severe cold deformation could increase its dislocation density to 10^{10} and even to $10^{11}/\text{cm}^2$ [16]. It can be seen from Figure 2 that the dislocation density in the grains of the AISI 304 SS obviously increased because of the expansion deformation. The quantitative relationship between corrosion current and dislocation density given by Gutman is shown in Equation (1) [17]:

$$\Delta i_{\alpha} = i_{\alpha} \left(\exp \frac{n\Delta\tau}{\alpha R'T} - 1 \right) \quad (1)$$

In Equation (1), Δi_{α} is the increase in anode current caused by plastic deformation, n is the number of dislocations contained in the dislocation up-pipe group, $\Delta\tau$ is the shear stress caused by up-pipe dislocation and T is the ambient temperature. It is not difficult to see that the anodic dissolution current density increases with an increase in the dislocation density, which explains the deterioration of the corrosion resistance of the AISI 304 SS tube in this work. In our research, the corrosion current density increased from 0.97 to 2.93 $\mu\text{A}\cdot\text{cm}^{-2}$, the capacitance arc radius decreased from 15,262 to 6766 $\Omega\cdot\text{cm}^2$ in the EIS and the corrosion rate increased from 0.018 to 0.0224 mm/a.

Researchers believe that the crystal defects caused by plastic deformation are the main reason for the reduction in the corrosion resistance of SS [16]. The mechanical twins and strain-induced martensite formed during plastic deformation can also affect the corrosion behavior of SS, as well as causing an increase in the dislocations. The corrosion behavior of two types of 304 SS after uniaxial tensile deformation was studied by Jafar [4]. In his study, the austenite stability in 304 SS was improved by using 2% Cu instead of 2% Ni, and the stain-induced martensite transformation during tensile deformation was completely suppressed. The 304 SS containing 2% Cu was still single-phase austenite after uniaxial tensile testing, whereas the volume fraction of strain-induced martensite in common 304 SS was more than 70%. The corrosion properties of the two types of 304 SS after uniaxial tensile testing were tested in a 3.5% NaCl solution. The results showed that the corrosion rate of 304 SS containing 70% martensite was twice that of single-phase austenite 304 SS. Therefore, Jafar suggested that strain-induced martensite is the main reason for the reduced corrosion resistance in 304 SS [4]. The adverse effects of strain-induced martensite on the corrosion

resistance of 304 SS have also been reported by Lou et al. [18]. However, in this study, not only was strain-induced martensite found in the microstructure of the AISI 304 SS after expansion, but a large number of mechanical twins were also observed in its deformed microstructure. The influence of cold deformation on the corrosion behavior of selective laser-melted 316L SS in a simulated cathode environment for proton exchange membrane fuel cells was studied by Ma et al. [19]. They stated that the mechanical twins caused by plastic deformation were conducive to improving the corrosion resistance of 316L SS when the strain was less than 50%. Moreover, Chen et al. reported that the intergranular corrosion resistance of AISI 304 SS could be improved with a high-density twinned structure, which was introduced into the microstructure of AISI 304 SS using mechanical attrition treatment of the surface, and the potentiodynamic polarization results showed that twinned 304 SS possessed higher E_{corro} and lower I_{corro} values than the sensitized and the as-received 304 SSs [20]. As well as austenitic SS, the beneficial effects of a mechanical twin structure on the corrosion resistance of other steels have also been reported [21]. Wang et al. reported that the corrosion resistance of Fe-30Mn-3Si-3Al TWIP steel was obviously improved by the formation of a twin structure that reduced the high-angle boundary energy [22].

It can be concluded that the reduction in the corrosion resistance of the AISI 304 SS tube used in this study was mainly related to the multiplication of dislocations and the strain-induced martensite caused by expansion deformation. Fortunately, the corrosion resistance of the AISI 304 SS tube was only slightly worse because of the limited strain, as shown by the corrosion simulation test in an autoclave. The corrosion resistance of the expanded AISI 304 SS tube still showed great natural advantages compared to the common casings, and its corrosion rate was only half that of the common casings; moreover, no pitting corrosion occurred on the surface of the AISI 304 SS specimens. In summary, the AISI 304 SS tube showed good comprehensive performance and is suitable for use as a SET under the working conditions proposed in this study.

5. Conclusions

The influences of expansion deformation on the mechanical properties and corrosion resistance of an AISI 304 SS tube in water from an oilfield were systematically studied in this work. Several conclusions can be drawn:

- (1) The expansion pressure of an AISI 304 SS tube with dimensions of $\phi 108 \text{ mm} \times 6 \text{ mm}$ was below 23 MPa when the expansion rate of the inner diameter was $\sim 11\%$. The final internal pressure and collapse strength of the tube after expansion were 71 and 32 MPa, respectively;
- (2) Multiplication of dislocations, strain-induced martensite transformation and twinning could be observed in the microstructure of AISI 304 SS tube after $\sim 11\%$ expansion deformation, which directly led to an increase in the strength and hardness of AISI 304 SS and a decrease in its elongation and impact toughness;
- (3) Expansion deformation led to an increase in the corrosion current density of AISI 304 SS in oilfield water, a decrease in the capacitive reactance arc radius in the EIS and an increase in the corrosion rate, which indicate a decline in the corrosion resistance of the steel. However, no obvious pitting corrosion features could be observed;
- (4) The deterioration of the corrosion resistance of the AISI 304 SS tube used in this research was mainly related to the multiplication of dislocations and the strain-induced martensite caused by expansion;
- (5) SETs manufactured from AISI 304 SS meet the requirements for repairing casing damage in conventional oil wells in terms of expansion pressure, mechanical strength and corrosion resistance.

Author Contributions: Conceptualization, X.R.; Formal analysis, D.L.; Investigation, J.Y.; Methodology, X.R. and D.L.; Supervision, W.Y.; Validation, L.H.; Writing—original draft, D.L.; Writing—review & editing, J.Y. All authors have read and agreed to the published version of the manuscript.

Funding: This work was supported by the Basic Research and Strategic Reserve Technology Research of PetroChina Company Limited (No. 2018Z-03), the Scientific Research and Technology Development

Project of PetroChina Company Limited (No. 2017F-19) and the Special Support Program for High Level Talents of Shaanxi Province (No. 00439).

Institutional Review Board Statement: Not applicable.

Informed Consent Statement: Not applicable.

Data Availability Statement: Not applicable.

Conflicts of Interest: The authors declare no conflict of interest.

References

1. Seibi, A.C.; Al-Hiddabi, S.; Pervez, T. Structural behavior of a solid tubular under large radial plastic expansion. *J. Energy Resour. Technol.* **2005**, *127*, 323–327. [\[CrossRef\]](#)
2. Pervez, T.; Qamar, S.Z.; Seibi, A.C.; Al-Jahwari, F.K. Use of SET in cased and open holes: Comparison between aluminum and steel. *Mater. Des.* **2008**, *29*, 811–817. [\[CrossRef\]](#)
3. Li, Y.; Lu, Z.; Li, T.; Li, D.; Lu, J.; Liaw, P.K.; Zou, Y. Effects of surface severe plastic deformation on the mechanical behavior of 304 stainless steel. *Metals* **2020**, *10*, 831. [\[CrossRef\]](#)
4. Jafari, E.J. Corrosion behaviors of two types of commercial stainless steel after plastic deformation. *Mater. Sci. Technol.* **2010**, *26*, 833–838. [\[CrossRef\]](#)
5. Kumar, B.R.; Singh, R. Effect of texture on corrosion behavior of AISI 304 stainless steel. *Mater. Charact.* **2005**, *54*, 141–147. [\[CrossRef\]](#)
6. Ali, H.; Abbas, N.; Ahmad, K.; Farnoosh, F. The effect of cold rolling regime on microstructure and mechanical properties of AISI 304L stainless steel. *J. Mater. Process. Technol.* **2010**, *210*, 1017–1022.
7. Sabooni, S.; Karimzadeh, F.; Enayati, M.H.; Ngan, A.H.W. The role of martensitic transformation on bimodal grain structure in ultrafine grained AISI 304L stainless steel. *Mater. Sci. Eng. A* **2015**, *636*, 221–230. [\[CrossRef\]](#)
8. Ingmar, B.; Marius, H.; Ilya, B.; Jorg, T.; Bernd, K.; Jérémy, E.; Michael, B. The influence of microstructure deformation on the corrosion resistance of cold formed stainless steel. In *MATEC Web of Conferences*; EDP Sciences: Les Ulis, France, 2018; Volume 190, p. 04002.
9. Ralston, K.D.; Birbilis, N. Effect of Grain Size on Corrosion: A Review. *Corrosion* **2010**, *66*, 075005. [\[CrossRef\]](#)
10. Gollapudi, S. Grain size distribution effects on the corrosion behaviour of materials. *Corro. Sci.* **2012**, *62*, 90–94. [\[CrossRef\]](#)
11. Moshtaghi, M.; Safyari, M. Effect of work-hardening mechanisms in asymmetrically cyclic-loaded austenitic stainless steels on low-cycle and high-cycle fatigue behavior. *Steel Res. Int.* **2021**, *92*, 2000242. [\[CrossRef\]](#)
12. Idrissi, H.; Renard, K.; Ryelandt, L.; Schryvers, D.; Jacques, P.J. On the mechanism of twin formation in Fe-Mn-C TWIP steels. *Acta Mater.* **2010**, *58*, 2462–2476. [\[CrossRef\]](#)
13. Karaman, I.; Sehitoglu, H.; Gall, K.; Chumlyakov, Y.I.; Maier, H.J. Deformation of single crystal hadfield steel by twinning and slip. *Acta Mater.* **2000**, *48*, 1345–1359. [\[CrossRef\]](#)
14. Karaman, I.; Sehitoglu, H.; Chumlyakov, Y.I.; Maier, H.J.; Kireeva, I.V. Extrinsic stacking fault and twinning in Hadfield manganese steel single crystals. *Scripta Mater.* **2001**, *44*, 337–343. [\[CrossRef\]](#)
15. Barbucci, A.; Cerisola, G.; Carbot, P.L. Effect of cold-working on the passive behavior of 304 stainless steel in sulfate media. *J. Electrochem. Soc.* **2002**, *149*, B534–B542. [\[CrossRef\]](#)
16. Xu, C.C.; Zhang, X.S.; Hu, G. Microstructure change of AISI 304 stainless steel in the course of cold working. *J. Beijing Univ. Chem. Technol.* **2002**, *29*, 27–31. (In Chinese)
17. Gutman, E.M. *Mechanochemistry of Solid Surface*; World Scientific: Singapore, 1994.
18. Luo, H.; Su, H.; Ying, G.; Dong, C.; Li, X. Effect of cold deformation on the electrochemical behaviour of 304L stainless steel in contaminated sulfuric acid environment. *Appl. Surf. Sci.* **2017**, *425*, 628–638. [\[CrossRef\]](#)
19. Ma, J.W.; Zhang, B.C.; Fu, Y.; Hu, X.J.; Cao, X.F.; Pan, Z.M.; Wei, Y.; Luo, H.; Li, X.G. Effect of cold deformation on corrosion behavior of selective laser melted 316L stainless steel bipolar plates in a simulated environment for proton exchange membrane fuel cells. *Cor. Sci.* **2022**, *201*, 110257. [\[CrossRef\]](#)
20. Chen, A.Y.; Hu, W.F.; Wang, D.; Zhu, Y.K.; Wang, P.; Yang, J.H.; Wang, X.Y.; Gu, J.F.; Lu, J. Improving the intergranular corrosion resistance of austenitic stainless steel by high density twinned structure. *Scr. Mater.* **2017**, *130*, 264–268. [\[CrossRef\]](#)
21. Kumar, M.; Schwartz, A.J.; King, W.E. Microstructural evolution during grain boundary engineering of low to medium stacking fault energy fcc materials. *Acta Mater.* **2002**, *50*, 2599–2612. [\[CrossRef\]](#)
22. Wang, K.; Wei, A.P.; Tong, X.; Lin, J.X.; Jin, L.F.; Zhong, X.T.; Wang, D. Improvement of the anti-corrosion property of twinning-induced plasticity steel by twin-induced grain boundary engineering. *Mater. Lett.* **2018**, *211*, 118–121. [\[CrossRef\]](#)